Springer

KSME

Journal of Mechanical Science and Technology 29 (1) (2015) 17~21
www.springerlink.com/content/1738-494x
DOI 10.1007/s12206-014-1203-2

AE analysis of delamination crack propagation in carbon fiber-reinforced polymer materials †

Sang-Jae Yoon[1], Dingding Chen[2], Seung-Wook Han[3], Nak-Sam Choi[4] and Kazuo Arakawa[1,*]

[1]*Research Institute for Applied Mechanics, Kyushu University, Kasuga-koen 6-1, kasuga, Fukuoka, 816-8580, Japan*
[2]*College of Basic Education for Commanding Officers, National University of Defense Technology, 410073 Changsha, China*
[3]*Department of Mechanical Engineering, Graduate School, Hanyang University, Seongdong, Seoul, 133-791, Korea*
[4]*Department of Mechanical Engineering, Hanyang University, Sangrok, Ansan, 426-791, Korea*

(Manuscript Received April 1, 2014; Revised May 23, 2014; Accepted June 2, 2014)

Abstract

Delamination fracture behavior was investigated using acoustic emission (AE) analysis on carbon fiber-reinforced polymer (CFRP) samples manufactured using vacuum-assisted resin transfer molding (VARTM). CFRP plate was fabricated using unidirectional carbon fiber fabric with a lay-up of six plies $[+30/-30]_6$, and a Teflon film was inserted as a starter crack. Test pieces were sectioned from the inlet and vent of the mold, and packed between two rectangular epoxy plates to load using a universal testing machine. The AE signals were monitored during tensile loading using two sensors. The average tensile load of the inlet specimens was slightly larger than that of the vent specimens; however, the data exhibited significant scattering due to non-uniform resin distribution, and there was no statistically significant different between the strength of the samples sectioned from the inlet or outlet of the mold. Each of the specimens exhibited similar AE characteristics, regardless of whether they were from the inlet or vent of the mold. Four kinds of damage mechanism were observed: micro-cracking, fiber–resin matrix debonding, fiber pull-out, and fiber failure; and three stages of the crack propagation process were identified.

Keywords: Acoustic emission (AE) analysis; CFRP composite; Damage mechanism; VARTM process

1. Introduction

Laminated composite materials have been applied in a variety of structural engineering fields, including aerospace, wind power plants, and the automotive industry. Conventional composite parts are typically manufactured using an autoclave method with unidirectional pre-preg composite fibers; however, autoclaves incur substantial installation costs and it is difficult to fabricate composite parts with complex shapes. Vacuum-assisted resin transfer molding (VARTM) is a composite fabrication process in which a thermoset resin is injected into a mold through inlet ports, and the core materials contained in the mold are saturated with the resin. This process can save both cost and processing for curing compared with the autoclave method because high pressures and temperatures are not required, and complex parts can be fabricated to reduce the number of parts required [1]. For these reasons, VARTM has become an increasingly popular method to fabricate carbon fiber-reinforced polymer (CFRP) parts.

The Research Institute for Applied Mechanics of Kyushu University in Japan has developed a new wind-lens turbine to generate high output power using a diffuser [2]. The research group plans to increase the size of the wind-lens turbine to a 5-MW class. The parts required for this are very large, and the wind turbine is composed of many curved components. The VARTM process is a promising method to fabricate these parts.

The VARTM process has three basic steps: fiber impregnation, consolidation (i.e., the application of pressure), and curing [3]. In this process, the contact quality of all layers is influenced by several factors, including the mold temperature, fiber orientation, resin viscosity, and pressure in the mold [4-8]. However, significant defects may occur depending on the local pressure gradient and permeability of the fabrics in the mold [9]. Moreover, incomplete filling of the resin may degrade the mechanical properties of the product due to the creation of voids and other non-uniformities in the resin distribution. Therefore, it is important to determine the optimal resin flow and to control the resin flow, as well as to investigate the causes of defects.

Various studies have reported optimal VARTM process conditions. Johnson [9, 10] applied an induction heating

*Corresponding author. Tel.: +81 92 583 7761, Fax.: +81 92 583 3947
E-mail address: k.arakaw@riam.kyushu-u.ac.jp
† This paper was presented at the FEOFS 2013, Jeju, Korea, June 9-13, 2013.
Recommended by Guest Editor Jung-Il Song

Table 1. Maximum load prior to failure for each specimen.

Specimen type	No.	Maximum force (N)	Specimen type	No.	Maximum force (N)
Inlet	1	216	Vent	1	222
	2	192		2	199
	3	207		3	213
	4	239		4	209
	5	210		5	187
	Average	212.8		Average	206

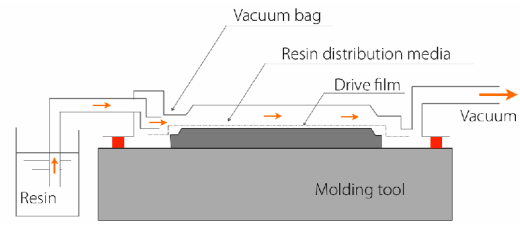

Fig. 1. Schematic diagram showing the VARTM process.

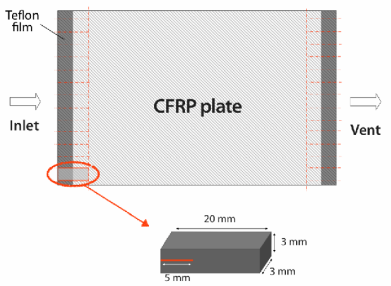

Fig. 2. Illustration showing where the specimens were sectioned from the CFRP plate.

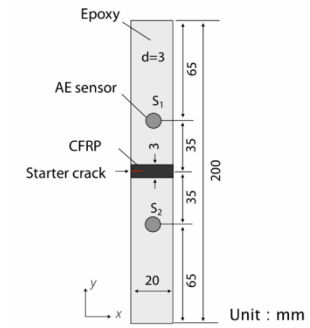

Fig. 3. Experimental tensile testing and AE monitoring procedures.

method to reduce the viscosity of the resin, thereby counteracting the effects of localized regions of low permeability, and simulated active flow control during the mold filling stage. Bender [11] reported an automatic pressure control and flow rate feedback method employing computer control between the inlet and vent parts. Correia [12] described a simulation analysis for the flow, compaction, and permeability. Kuentzer [13] explored the resin bleeding and flow resistance of the void content within fiber tows experimentally and via numerical simulations. Lee [14] investigated the effects of the fiber direction on the resin flow direction. However, most of these studies focused on process control. The effects of non-uniformities on the mechanical properties of the VARTM-formed composite materials have not been investigated in detail.

Here, we describe the results of a study of the effects of non-uniformities on composite materials by forming CFRP plates using VARTM. Specimens for tensile testing were formed with a starter crack inserted in the CFRP plate, and sections were examined from the inlet and vent of the mold. Acoustic emission (AE) signals were monitored during the tensile fracture tests. The fracture surface was observed following the tests, and the AE characteristics were analyzed to investigate the fracture behavior of the specimens. Three stages of the fracture behavior were identified from the amplitudes and frequency spectra of the AE signals.

2. Experimental procedure

2.1 VARTM process

Laminated composite specimens with a single edge notch were fabricated using the VARTM process. Fig. 1 shows the transverse flow VARTM setup, which is commonly employed in the fabrication of very large parts [1]. Unidirectional carbon-fiber fabrics (SAERTEX) were laid up in a one-side mold with a sequence of $[+30/-30]_6$. Teflon film was inserted as a starter crack in two edges of the plate, as shown in Fig. 2. The fabrics were sealed in a vacuum bag, and then the resin (Nagase ChemetX) was impregnated into the fiber layers using the vacuum. The process was carried out at room temperature.

2.2 Tensile specimens

To fabricate the tensile test specimens, ten pieces were sectioned from the inlet and vent of the plate, as shown in Fig. 2. The pieces were packed between two rectangular epoxy plates to clamp the specimens to a universal tensile testing machine (Zwick 250, testXpert), as shown in Fig. 3.

3. Results and discussion

3.1 Tensile fracture test and AE analysis

Figs. 4(a) and (b) show typical tensile loads and amplitudes of the AE signal as functions of time for the specimens sectioned at the inlet and vent of the mold, respectively. The tensile loads are listed in Table 1. Although the average tensile load of the inlet (212.8 N) was slightly larger than that of the vent (206 N), the data exhibited significant scattering, and as such, there was no statistically significant difference between the tensile strength of the parts formed at the inlet and the vent. Johnson [8, 9] suggested that mold-filling during VARTM is a

Table 2. Amplitude and peak frequency of the AE signals during each stage.

Stage	Amplitude (mV)	First peak frequency (kHz)
I	5 - 50	130 - 170
II	10 - 40	150 - 250
III	500 - 10000	120 - 250

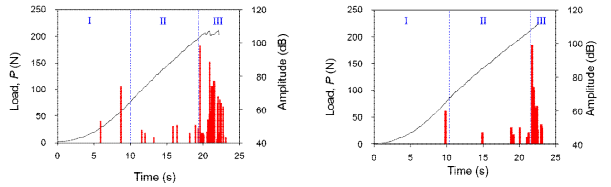

(a) (b)

Fig. 4. Load-displacement curves and the corresponding AE amplitudes as a function of time for specimens sectioned from (a) the inlet; (b) the vent regions of the mold.

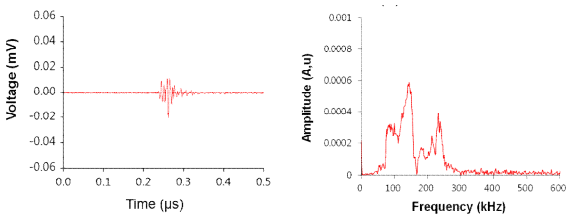

(a) (b)

Fig. 5. Burst-type AE signals during stage I of fracture: (a) waveform; (b) frequency spectrum.

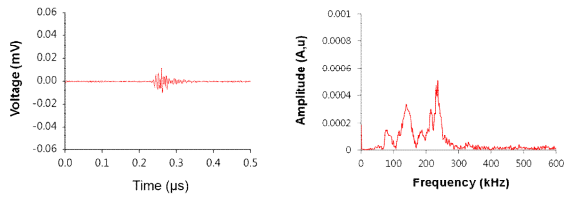

(a) (b)

Fig. 6. Burst-type AE signals during stage II of fracture: (a) waveform; (b) frequency spectrum.

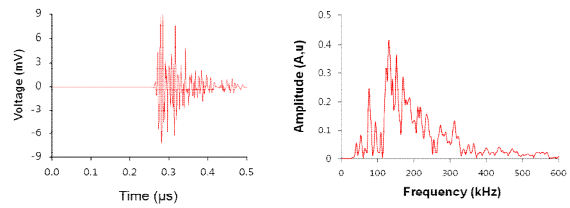

(a) (b)

Fig. 7. Burst-type AE signals (with a large amplitude) during stage III of fracture: (a) waveform; (b) frequency spectrum.

critical step in the process, and that defects often arise in regions of local low permeability, or in regions that are too far from the inlet or vent. The variation in the tensile strength may

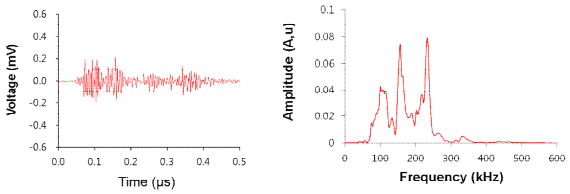

(a) (b)

Fig. 8. Continuous AE signals during stage III: (a) waveform; (b) frequency spectrum.

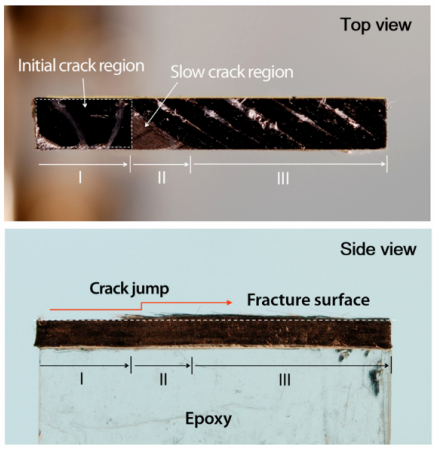

Fig. 9. Optical microscopy image of a fracture surface.

also be affected by non-uniformities of the fabrication process. The specimens exhibited similar AE characteristics, regardless of whether they were sectioned from the inlet or vent of the mold. Based on these data, we were able to identify three stages of the fracture behavior, which will be discussed in the following subsection.

3.2 Fracture mechanism

The AE signals were analyzed in the time domain, as well as the frequency domain through the use of fast Fourier transforms (FFTs) of the time domain AE amplitudes. Figs. 5-8 show typical amplitude and frequency spectra of the AE signals during each stage of failure. Most of the AE signals exhibited a burst-type signal during fracture or crack growth, although continuous-type signals were observed during stage III (see Fig. 8). It should be noted that the crack propagation was significantly faster during stage III. Table 2 lists the distribution of the amplitudes and the frequency range of the lowest-frequency broad features in the AE signals. During stage I of failure, the samples exhibited low-amplitude AE signals, and most of the acoustic energy was at frequencies below 160 kHz. During stages II and III, the AE spectra exhibited wide bands at around 120–240 kHz.

Fig. 9 shows an optical microscopy image of a fracture surface. The three stages of crack propagation described above are marked on the fracture surface. During stage II, an area

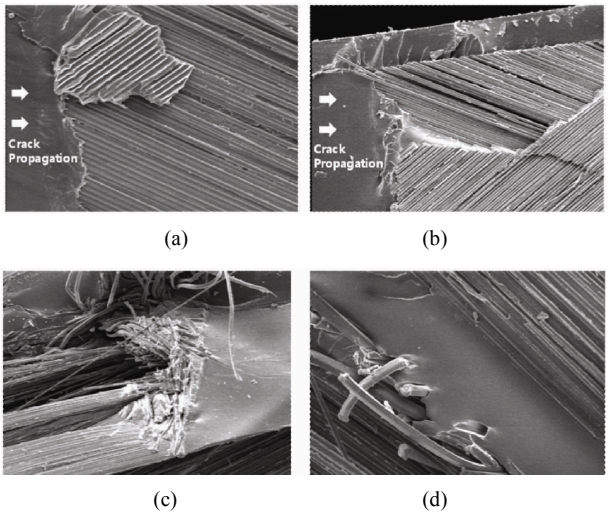

Fig. 10. SEM microscopy images of the fracture surfaces: (a) resin cracking; (b) fiber-matrix debonding; (c) fiber pull-out; (d) fiber failure.

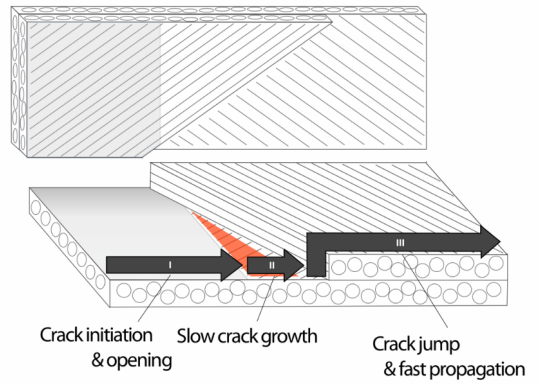

Fig. 11. Illustration of the fracture behavior in response to tensile loading.

corresponding to slow crack growth was observed. The fiber-bonded area was less than 80% delaminated opposite the fracture surface. This suggests that the matrix strength was stronger than the fiber-matrix strength, which corresponded to less than 80% of the bonded area.

At start of stage III, the crack propagation route changed to another layer. This stage was marked by a significant increase in the AE amplitudes (see Fig. 7). It follows that much energy was stored during the slow crack propagation of stage II, and that the crack suddenly jumped to the other layer, releasing a large amount of energy.

To further investigate the damage mechanism and to understand the relationship with the frequency spectra of the AE signals, scanning electron microscopy (SEM) images of the fracture surfaces were obtained. Fig. 10 shows four typical fracture phenomena at the fracture surface of the specimens, and Table 3 lists the phenomena that occurred during each stage. From a comparison with Table 2, the frequency band below 160 kHz appears to correspond to matrix-related fracture, and frequencies above 160 kHz correspond to fiber-related fracture.

Table 3. Observed damage mechanisms during each stage.

Stage	Phenomena
I	Resin cracking
II	Resin cracking, fiber-matrix debonding
III	Resin cracking, fiber-matrix debonding, fiber pull out, fiber failure

The fracture behavior during the three stages is illustrated in Fig. 11 based on the AE and fracture surface observations. During stage I, the crack initiated, opening up along the starter crack. Since the resin permeated into the starter crack interface during specimen fabrication, the starter crack closed due to the hardened resin. During stage II, the crack reached a poor adhesion area located at end of the starter crack. The crack propagated slowly until it reached fibers with at least ~80% of degree of adhesion. The crack propagation was temporarily restrained, and the strain energy accumulated at the crack tip. During stage III, the stress intensity factor reached the fracture toughness, and the crack suddenly jumped to another layer, and then propagated rapidly with a large strain energy release rate. During stage III, numerous fracture mechanisms occurred, and the AE spectra indicated a large strain-energy release rate.

4. Conclusions

Property non-uniformities of CRFP samples formed using VARTM were investigated using tensile testing and AE spectra. The tensile tests showed that average load of the inlet specimens was higher than that of the vent specimens; however, the data exhibited significant scattering, which was attributed to non-uniformities in the distribution of the resin, and the difference between the properties of the inlet and vent was not statistically significant. The AE spectra of each specimen were similar, regardless of whether they were taken from the inlet or vent of the mold.

The fracture behavior of the VARTM-formed CFRP material was investigated under tensile load. Failure could be classified into three stages: (i) crack initiation and opening along the starter crack (with an AE amplitude of 5-50 mV and a frequency spectrum of 130–160 kHz), (ii) slow crack growth (10–40 mV and 160–240 kHz), and (iii) rapid propagation (500–10000 mV and 120–240 kHz).

Acknowledgment

This work was partly supported by a research grant from the Japan Society for Promotion of Science (#26630496), and by the Collaborative Research Program of Research Institute for Applied Mechanics, Kyushu University.

References

[1] Y. Rachmadini, V. TAN and T. TAY, Enhancement of mechanical properties of composites through incorporation

of CNT in VARTM - A review, *J Reinf Plast Comp*, 29 (18) (2010) 2782-2807.

[2] Y. Ohya and T. Karasudani, A shrouded wind turbine generating high output power with wind-lens technology, *Energies*, 3 (4) (2010) 634-649.

[3] A. Miravete, *Processing and manufacturing composite design tutorial*, Aero/Astro Department, Stanford University (2007).

[4] J. L. Zhao, T. Fu, Y. Han and K. W. Xu, Reinforcing hydroxyapatite/thermosetting epoxy composite with 3-D carbon fiber fabric through RTM processing, *Mater Lett,* 58 (2004) 163-168.

[5] J. F. Timmerman, B. S. Hayes and J. C. Seferis, Nanoclay reinforcement effects on the cryogenic microcracking of carbon fiber/epoxy composites, *Compos Sci Technol*, 62 (2002) 1249-1258.

[6] J. Bozza, M. Erdal and S. Guceri, Resin transfer molding of continuous fiber-reinforced, particle-filled ceramic–ceramic composites: particle filtration, *In: Proceedings of the 28th international SAMPE technical conference* (1996).

[7] A. Haque, M. Shamsuzzoha, F. Hussain and D. Dean, S2-glass/epoxy polymer nanocomposites: manufacturing, structures, thermal and mechanical properties. *J. Mater. Sci. Lett.,* 20 (2003) 1439-1441.

[8] S. W. Han, N. S. Choi and M. S. Lee, Analysis of glass fabric impregnation using a resin drop method, *J. Mech. Sci. Technol.*, 26 (5) (2012) 1477-1482.

[9] R. Johnson and R. Pitchumani, Enhancement of flow in VARTM using localized induction heating, *Compos Sci. Technol.*, 63 (15) (2003) 2201-2215.

[10] R. Johnson and R. Pitchumani, Flow control using localized induction heating in a VARTM process, *Compos Sci Technol*, 67 (3-4) (2007) 669-684.

[11] D. Bender, J. Schuster and D. Heider, Flow rate control during vacuum-assisted resin transfer molding (VARTM) processing, *Compos Sci Technol*, 66 (13) (2006) 2265-2271.

[12] N. Correia, F. Robitaille, A. C. Long, C. D. Rudd, P. Šimáček and S. G. Advani, Use of resin transfer molding simulation to predict flow, Saturation, and Compaction in the VARTM Process, *J Fluid Eng-T ASME*, 126 (2) (2004) 210-215.

[13] N. Kuentzer, S. Pavel, S. G. Advani and S. Walsh, Correlation of void distribution to VARTM manufacturing techniques, *Compos Part A-Appl S*, 38 (3) (2007) 802-813.

[14] L. Y. Lin, H. J. Lee, C. E. Hong, G. H. Yoo and S. G. Advani, Preparation and characterization of layered silicate/glass fiber/epoxy hybrid nanocomposites via vacuum-assisted resin transfer molding (VARTM), *Compos. Sci. Technol.*, 66 (13) (2006) 2116-2125.

Sang-Jae Yoon is a research fellow of the Research Institute for Applied Mechanics, Kyushu University, Japan. He received his Dr. Eng. degree from Kyushu University in 2014. His research interests include advanced composite materials, acoustic emission analysis and fracture behavior of engineering materials.

Kazuo Arakawa Kazuo Arakawa is a professor of the Research Institute for Applied Mechanics, Kyushu University, Japan. He received his Dr. Eng. degree from Osaka University in 1982. He stayed at University of Washington as a visiting researcher from 1988-1989. He has published over 200 papers in Japanese and International Journals on solid mechanics including fracture mechanics on polymers and composite materials, dental biomaterials, and impact phenomena of golf balls. He has received many academic awards including the Technology Award, the Best Paper Award from the Japanese Society of Experimental Mechanics and so on.